HEALTH MONITORING FOR SPACECRAFT REACTION WHEELS

Daniel Bojiloff [(1)], Tobias Häfner [(2)], René Seiler [(3)]

[(1)]ESA/ESTEC, Keplerlaan 1, NL-2201 AZ Noordwijk, The Netherlands, Email: daniel.bojiloff@esa.int
[(2)]ESA/ESTEC, Keplerlaan 1, NL-2201 AZ Noordwijk, The Netherlands, Email: tobias.haefner@esa.int
[(3)]ESA/ESTEC, Keplerlaan 1, NL-2201 AZ Noordwijk, The Netherlands, Email: rene.seiler@esa.int

Abstract

In order to reduce fuel consumption and extend the lifetime of the INTEGRAL spacecraft, a new operation scheme for the reaction wheels was proposed. The new operation at low wheel speeds may potentially impair RW performance. Therefore an investigation is being conducted at ESTEC. The investigation consists of hardware testing on the flight spare wheel, in-flight testing on the INTEGRAL spacecraft and performance modelling and simulation. The tests showed that up to now, after 9 months of low speed operation, there is no indication of performance degradation caused by low speed operation. The in-flight tests demonstrated a sufficiently good pointing stability employing the new scheme. The simulation activities shed some light on the composition of torque losses. However, some aspects are yet to be investigated and the investigation shall continue to build up confidence in the new scheme.

1 Introduction

Over the past years, the long-term-stability of space mechanisms has been investigated at ESTEC in close cooperation with ESOC and industrial partners on numerous occasions. A recent example of such an investigation is the performance monitoring activity tied to the INTEGRAL (International gamma-ray astrophysics laboratory) mission. In 2015 the end of life of the INTEGRAL spacecraft was predicted for 2021 due to fuel depletion. A proposal was made by ESOC which encompasses several fuel saving measures in order to prolong the spacecraft's lifetime by approximately 8 years. Given the preciousness of science time on this high profile space observatory, the proposal is deemed highly attractive. However, some aspects of the proposed operation scheme may negatively affect the reaction wheels (RWs). Those will be required to run at speeds below a minimum speed requirement (65 rpm) as defined by the manufacturer. Such a requirement is commonly imposed on the RWs in order to guarantee a stable lubricant film thickness in the bearings which is, amongst others, dependent on speed. Insufficient or unstable film thickness may lead to metal-on-metal contact between bearing balls and races and thus to increased friction and wear.
INTEGRAL is supposed to employ this new scheme until end of mission which is foreseen for 2029. In order to adequately assess the risks related to long term low speed operation, a thorough investigation is necessary.
The study roadmap is comprised of three main pillars on which confidence in the new scheme shall be built:

1. Hardware test activities in the Mechanisms Test Facility at ESTEC, using the INTEGRAL flight spare RW and complementary tests on ball bearing unit level performed at Bradford Engineering BV.

2. On-orbit testing (performed by ESOC) and analysis of in-flight telemetry data to fully understand the operational changes and their impacts on operations.

3. Establishment of a computer-based performance model for the simulation of relevant operating principles & underlying physical effects (using MATLAB®/ Simulink® and ANSYS Maxwell®)

Conducting this investigation, we hope to shed light on how performance and wear of RWs evolve during long term low speed operation.

2 Hardware test activities

The hardware test activities were conducted in close cooperation with Bradford Engineering BV. Dedicated low speed operation tests were performed at Bradford Engineering BV on bearing unit level. Tests on reaction wheel assembly (RWA) level were conducted at ESTEC.

2.1 RWA level health monitoring

The RWA tests are comprised of long term low speed operation phases and reoccurring health checks (HCs), during which the low speed operation is interrupted in order to perform a set of standard tests to assess RW health status. The RW was suspended with a horizontal spin axis during the low speed operations and most health check procedures. A Honeywell torque transducer Model 2102-50 was used to measure reaction torques in that configuration. This sensor was calibrated and

characterised with the RW attached to ensure accurate measurement readings and a linear sensor behaviour. The wheel was mounted with a vertical rotation axis on a Kistler table for microdynamic measurements. Both arrangements are shown in figure 2-1.

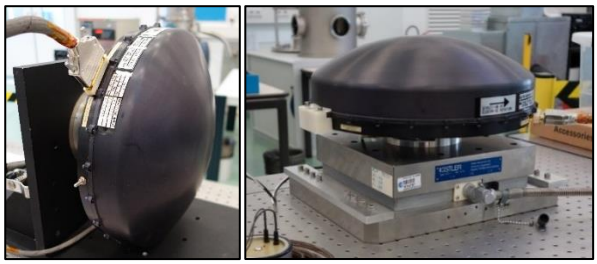

Figure 2-1: Integral flight spare reaction wheel on torque transducer (left) and on Kistler table (right)

The torque transducer's measurement range extends from 0 to 5 Nm. The Kistler table measures forces from few mN to 20 kN in the frequency range between 50 and 5000 Hz.
To simulate a worst case of low speed operations, the wheel speed was varied between 10 rpm CW and CCW, at steps of 1rpm per hour. This profile was applied for 280 days. Due to controller and tacho limitations, a reasonably stable velocity could only be achieved above 4 rpm. Below that threshold, the wheel speed is unstable. Although different control laws are used, a similar behaviour is observed on-orbit. The resulting operation profile can therefore be regarded as representative. Throughout the campaign, reaction torque and wheel telemetry was logged with a sampling rate of 10 Hz. In the beginning, after 3 months and at the end, health checks (HC1, 2 and 3) where performed. Those encompassed 5 standardised tests which were developed by the manufacturer to measure functional parameters, parasitic/ loss torque and potentially irregular behavior. During HC1 and HC3, microvibrations of the wheel were measured. The comparison of these three HCs revealed only minor changes.

Statistical Assessment of Loss Torque:

Loss torque is used to monitor the behaviour of the wheel and especially its bearings during operations. It is estimated using motor current, motor constant and reaction torque. For every hourly speed step, the 10 Hz torque data is compressed into the four statistical moments mean, variance, skewness and kurtosis. Figure 2-2 depicts an excerpt of the statistical data. The wheel shows a lively, but long term stable behaviour during such low speed operations. Detailed analysis shows, the variations are mainly linked to one specific engine order related to outer ring imperfections. This imperfection was present from the beginning, no trends or changes are seen over the course of the campaign.

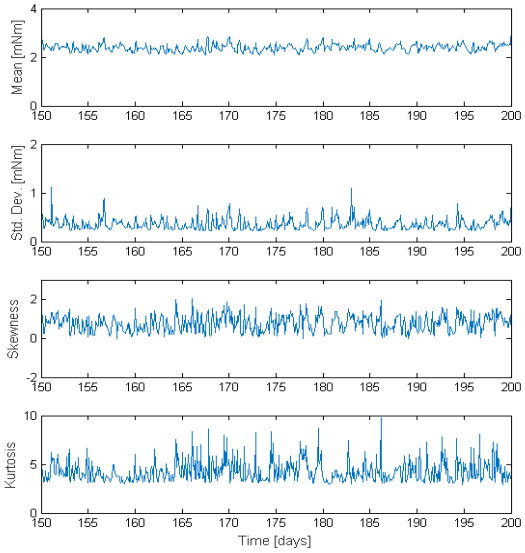

Figure 2-2 Low speed loss torque monitoring

Stiction Torque:

Stiction torque was measured with a dedicated test during the health checks. The mean stiction torque was calculated to 5.39 mNm during HC1. The maximum and minimum values measured were 7.27 mNm respectively 4.26 mNm, which is within the expected range for this wheel type. During HC2 and HC3, no significant change in stiction behaviour was observed.
Additionally, stiction torque was recorded at every start-up after a zero crossing during low speed operations. After the first month, some zero crossings showed increased stiction with typical values around 30 mNm, and a maximum of 50 mNm. The phenomenon appeared randomly at about 10% of the zero crossings and as such remained stable throughout the campaign. Because the phenomenon was not apparent during health checks, it can be interpreted as a feature, rather than as a degradation. It is presumably linked to the very low speeds and long stand still time at zero crossing.

Loss Torque Characteristic/Coefficient:

The plot below (cf. figure 2-3) shows the loss torque characteristic of the wheel obtained during HC1. This characteristic is of very high interest, as extreme aberrations from these curves could indicate significant performance degradation or even imminent RW failure.

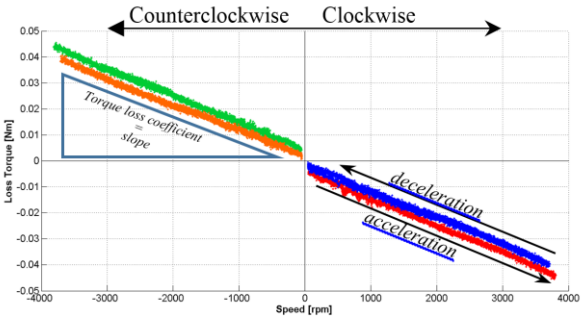

Figure 2-3 Results of the full speed full torque test

The slope of the above characteristic represents the torque loss coefficient (k-value). This value (around -1*10^{-4} Nm/rad/s) dropped by 1% in HC2 and by a further 2% in HC3.

Coulomb Friction:

The coulomb friction torques measured were ranging from 2.17 mNm to 2.46 mNm during HC1. These values dropped by approximately 20% from HC1 to HC2 and by approximately 26% from HC1 to HC3. A decrease in coulomb friction does not indicate performance degradation and could even be regarded beneficial. The specific values are shown in table 2-1.

Table 2-1: Coulomb friction torques for HC 1 to 3

	Coulomb Torque [mNm]		
	HC1	HC2	HC3
CW acceleration	2.30	1.82	1.69
CCW acceleration	2.40	1.93	1.78

The y-intercepts of the loss torque characteristic (cf. figure 2-3) should also yield the coulomb torque. Due to what is believed to be the sensor hysteresis, the values for acceleration and deceleration are wider spread. The maximum value obtained is 5.4 mNm (HC3) which is still in family with the estimated coulomb friction torque of almost identical wheels on the Rosetta spacecraft.

Irregular Behaviour:

The tests showed no significant spikes and leaps in torque and torque change rate during HC1 and HC2. During HC3 a temporary, but for the limited time stable increase in friction torque could be observed which might indicate cage instability. However, no conclusions regarding degradation of the wheel can be drawn from such an isolated event, since this wheel type is known for showing such peaks occasionally.

Microvibration Characteristics:

A multichannel Kistler dynamometer was used to record the forces and torques produced by the wheel during coast down from full speed to standstill. For these tests, a sampling rate of 12.8 kHz was used. Just comparing force magnitudes can lead to misinterpretations, as microvibrations are a combination of vibration sources and structural resonances. The latter often are not only linked to the item under test, but also to the test equipment. Small variations of resonances, which are difficult to control, can lead to big variations in measured peak forces. To identify and track vibration sources, waterfall diagrams as depicted in figure 2-4 are used.

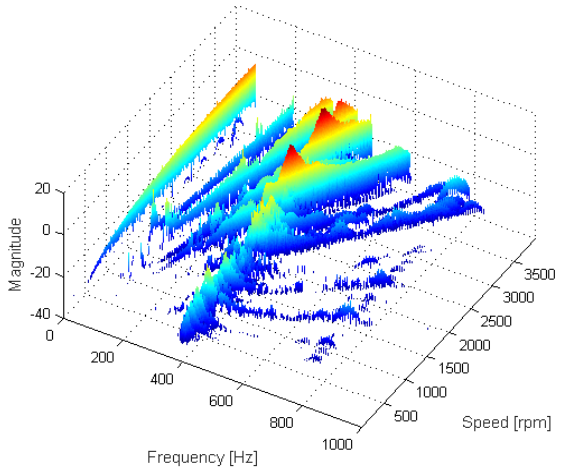

Figure 2-4 Integral flight spare RW waterfall plot

Engine orders, visible as rays pointing towards the origin, are linked to wheel and bearing features [1]. A main contributor to the signal is rotor imbalance. Engine orders linked to ball bearing cage, balls and inner / outer race imperfections are also clearly visible. They contain less energy than imbalance. When intersecting with structural resonances at distinct velocities, they nevertheless can become the major contributor to microvibrations. Rocking modes of the rotor are present, amplifying low number engine orders when intersecting with them at certain speeds.
Microvibrations were measured at HC1 and HC3, and bearing linked engine orders were compared. No significant change was observed.

High Resolution Order Analysis:

A high resolution order analysis was performed to identify more detailed features. For an order analysis, the vibration signal is resampled to a fixed angular increment of the rotating part. Therefore, an accurate tacho or angle measurement is essential. Subsequently, a fourier transformation is performed, transforming the signal

from angular domain to order domain. The maximum visible order depends on the angle increment, the order resolution depends on the sampling length.
In this case, a measurement over 2E5 revolutions was used, leading to an order resolution of 5E-6 $\frac{1}{rev}$. To do so, wheel speed was ramped from 2000 RPM to 500 RPM over 160 minutes. A variable speed ensures that any fixed frequency noise gets suppressed. For a proof of concept, changes in axial bearing load were detected with this technique. In the lab, those where enforced by changing the orientation of the wheel, hence adding or removing the weight of the rotor.
Several engine orders can be linked to the cage, as well as inner and outer race imperfections of the bearing. They follow equations 1, 2 and 3, with number of balls n, ball diameter d, pitch diameter D and contact angle α. Higher harmonics and side-orders are also visible [1].

$$H_{Cage} = \frac{1}{2}\left(1 + \frac{d}{D}\cos(\alpha)\right) \quad (1)$$

$$H_{IRI} = \frac{n}{2}\left(1 + \frac{d}{D}\cos(\alpha)\right) \quad (2)$$

$$H_{ORI} = \frac{n}{2}\left(1 - \frac{d}{D}\cos(\alpha)\right) \quad (3)$$

A change in preload induces a change of the contact angle. This relationship is not linear and is best determined using an FEA model or dedicated software like CABARET. For the investigated wheel and its soft preloaded bearings, adding the rotor weight changes the load, hence contact angle and order number, of one bearing. The other one remains unaffected.

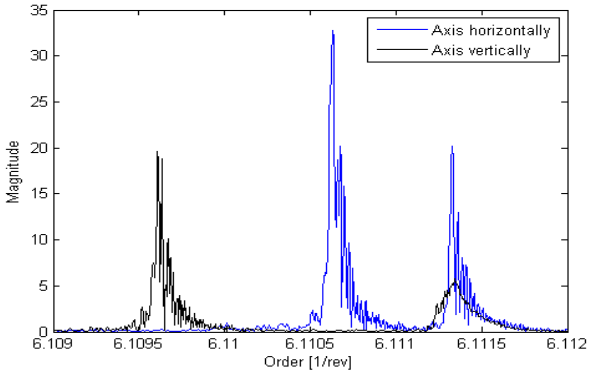

Figure 2-5 High resolution order analysis

As an example, figure 2-5 shows engine order 6.11 $\frac{1}{rev}$ in two different orientations. For each orientation, two peaks appear, representing each bearing with its unique real geometry. When adding or removing the rotor weight, the peak of one bearing is shifted. Table 2-2 shows the measured order shifts and calculated contact angle changes of the most prominent engine orders. The mean calculated angle change is 0.1951° with a standard deviation of 0.0029°. According to the CABARET model, that corresponds to a load change between 43N and 45N. The additional load due to nominal rotor mass would be 49.7 N.
Comparing high resolution order analysis data from HC1 and HC3, no obvious change in characteristics could be identified.

Table 2-2: High resolution order analysis

Feature	**Order [$\frac{1}{rev}$]**	**Δ order [$\frac{1}{rev}$]**	**Δ α [°]**
Cage	0.61	Ax: 1.04E-4 Rad: 0.99E-4	0.2015 0.1918
(ORI-2)/2	0.945	Ax: 5.07E-4 Rad: 5.02E-4	0.1961 0.1941
IRI/2	3.05	Ax: 5.01E-4 Rad: 5.01E-4	0.1938 0.1937
ORI	3.89	Ax: 9.99E-4 Rad: 9.95E-4	0.1932 0.1923
IRI	6.11	Ax: 1.017E-3 Rad: 1.022E-3	0.1966 0.1976

2.2 Bearing Unit Level

Test on ball bearing units, stemming from the original production batch for Integral, were conducted at Bradford Engineering BV. They revealed that there is almost no contribution of viscous friction torque. This is due to oil depletion in the ball bearings. How much oil exactly remained in the tested ball bearing unit and whether it is exactly as much as in the flight spare RW or the RWs in orbit is debatable. However, the fact that the initial lubrication was similar in all cases, the bearings were run for long periods of time in all cases and there is no indication of significant viscous losses in all cases leads to the assumption that the tested bearing unit and the flight spare RW are in conjunction sufficiently representative of the RWs on the INTEGRAL spacecraft with respect to the scope of this investigation.

3 On-Orbit Tests & TM Data assessment

5 on-orbit tests performed by ESOC in 2015 showed increased tacho noise between +6 and -6 rpm. This may be related to stick-slip-processes, tacho resolution and measurement rate, and controller behaviour. The increased noise did have a negligible effect on the pointing stability [2]. The new operation scheme therefore does not impair the quality of the gathered scientific data. The tests showed no negative effects on the RWs, however, they lasted only 8h each and are therefore not sufficient to assess the effects of long period low speed operation.

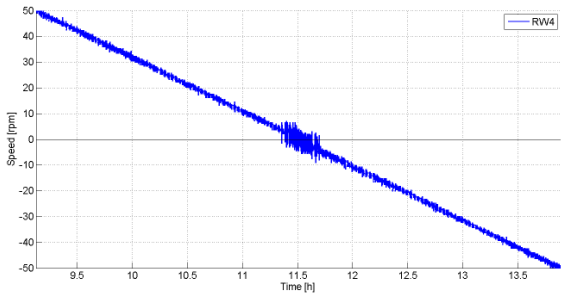

Figure 3-1 Wheel speed zero crossing on-orbit

4 Performance Modelling and Eddy Current Simulation

A RW performance model is under development which shall foster the understanding of processes in a RW by recreating certain phenomena (e.g. increased noise around zero crossing) and which allows to implement working theories into the model or to estimate effects of changing boundary conditions. A major building block in this activity is the correct representation of loss torque. The various contributors to loss torque are known, the share to which they contribute to overall loss torque however is not. The composition of loss torque was therefore identified to require further attention. Since eddy currents were assumed to be a major contributor to overall loss torque, a dedicated eddy current simulation was conducted using ANSYS Maxwell.

4.1 Performance Model in MATLAB/SIMULINK®

The Simulink model encompasses detailed building blocks for the controller, commutation logic, brushless dc motor, tachometer, rough thermal model, loss torque calculation, etc. The model was used to simulate the test profiles which were also used for the RWA health checks. By comparing simulated data and measurement data we showed that the computer model closely resembles the real RW in the test environment.

The proper representation of controller and tachometer in combination with a realistic loss torque characteristic including stiction is of special interest since these aspects are believed to be the root cause of increased noise around zero rpm. In order to accurately describe the loss torque contributors, a dedicated analysis of eddy current effects was performed.

4.2 Eddy Current Simulation in ANSYS Maxwell

The software tool ANSYS Maxwell® Version 17 was used for the electromagnetic modelling and simulation.

In the frame of this study, eddy current losses were simulated as a function of rotation speed and air gap size based on a simple model (disc rotating in the air gap of one magnet with two iron yokes), the influence of mechanical stiffener ribs was assessed using certain parts of a simplified reaction wheel design, and a eddy current loss torque vs speed characteristic was generated employing a detailed RW model. The obtained characteristic was fitted with a simple model approximation and the result was set in context with overall losses in the RW to assess the impact of eddy current induced loss torque. The influence of simulation step size and mesh quality were thoroughly investigated and the findings were considered in the simulation runs in order to gain confidence in the simulation results.

4.2.1 Simulation Results

A parametric study varying the reaction wheel's rotation speed from 0 to 4000 rpm using the simple model yielded a loss torque vs. speed characteristic, which is consistent with similar case studies found in literature, often in context of eddy current brakes. It is noteworthy that the maximum loss torque is already reached at about 2500 rpm and that an approximately linear behaviour is restricted to low speeds (<1000 rpm).
Simulations using simplified reaction wheel models showed the big influence of stiffening ribs on the baseplate below the electric motor of the particular reaction wheel design studied, manifested by strong oscillations and a higher mean value. This is due to the high dependency of eddy current induction on air gap dimensions. The effective (axial) air gap size is significantly reduced (by factor 2.4) at the location of the ribs.
It should be noted that only one-sixth segment of the whole assembly was modelled, taking advantage of the circular symmetry, in order to reduce the computational effort. The geometry representing the real RW assembly was used for the simulation, however fasteners, small holes, chamfers, etc. were removed.

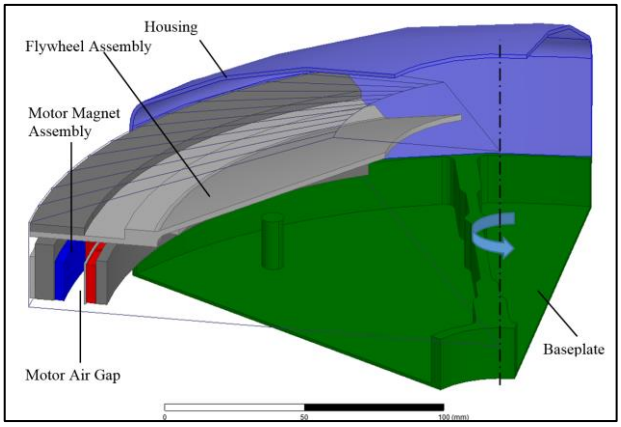

Figure 4-1: Detailed RW model

The validation of the model with respect to the magnetic properties was done in several steps. The magnetic field (H-field) and flux density (B-field) measurements on a single magnet were compared with the corresponding simulation data. Another element of model verification was done via comparison of the simulated magnetic flux density B at different locations in the detailed model and measured data, particularly in the motor air gap where approximately 0.4 Tesla are reached. The comparison showed a good match between measurement and simulation results, leading to the conclusion that the key features of the model, particularly the B-H characteristic of the magnets, are well defined. Based on figure 4-2 below, the propagation of the magnetic field was also assessed qualitatively and found consistent with the definition of motor pole pairs either side of the air gap.

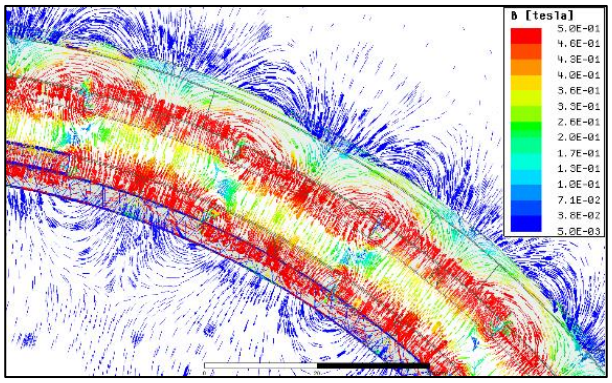

Figure 4-2: B-field vector plot of the motor airgap

After a series of numerical simulations which yielded the loss torque vs speed characteristic displayed in figure 4-3, a simplified model was used to approximate this characteristic. The curve fitting was done in MATLAB® based on equation (1), where ω is the rotational speed in rpm and T_{ECL} is the eddy current induced loss torque in Nm. The model equation has been suggested in the context of eddy current brakes [3]. The fitting process yielded model coefficients α, β and γ as shown below.

$$T_{ECL} = \gamma(e^{-\beta\omega} - e^{-\alpha\omega}) \qquad (4)$$

$$\alpha = 0.000115\frac{1}{rpm} \qquad \beta = 0.000868\frac{1}{rpm}$$

$$\gamma = -0.004685 \text{ Nm}$$

The final characteristic and the simple model approximation are shown in figure 4-3 below. The residual uncertainty of the simulation results caused by a selected step size, mesh quality limitations and any imperfections of the model w.r.t. the real RW hardware is estimated with approximately 10%.

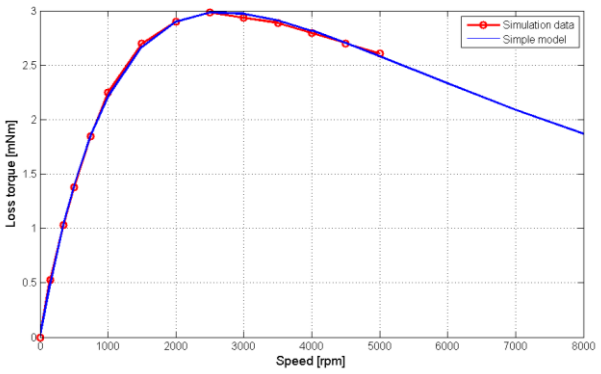

Figure 4-3: Simple model approximation

4.3 Further Use of the Results and Conclusions

As a main result, the simplified model according to equation (4) was used as input for the reaction wheel overall performance model implemented in Simulink®. Figure 4-4 depicts the composition of the total loss torque for the particular reaction wheel type investigated. It is concluded that eddy current induced losses are not dominating the total loss torque vs. speed characteristic. Evidently, there must be other substantial contributors to the loss torque at RW level, in order to explain the large remaining difference between the identified torque components and the measured (total) characteristic (cf. figure 4-4), which is surprisingly linear, regular and long-term stable. It has been already verified that viscous losses due to the mechanical bearings do not suffice to cover the discrepancy. Hence, the investigation will be continued with the aim to identify and quantify the missing loss torque components.
Apart from this, the study has revealed interesting side effects like the big impact of structural features (e.g. stiffening ribs) on eddy current related losses. These manifested in loss torque oscillations.

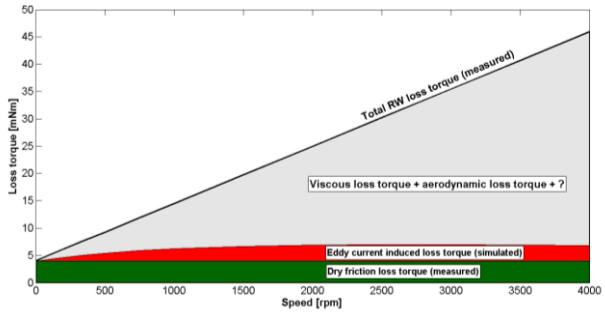

Figure 4-4: Assumed loss torque composition (for the Integral RW)

5 Conclusion

The comprehensive investigation approach taken for this activity shed light on the characteristics of this reaction wheel type and its behaviour at low speeds.
On-orbit tests have shown that the satellite and its AOCS system keep fulfilling the operational and pointing requirements with the proposed low speed operations [2].
The endurance test on ground has shown an overall stable behaviour without indications for increased wear of the bearings. Two long term effects have been identified: A decrease in coulomb friction of the bearing is presumably a run-in effect after the wheel has been stored for several years. An increased stiction torque at about 10% of the zero crossings could not be fully explained yet, but accompanying measurements indicate that this feature is linked to the distinct on-ground testing profile. Microvibration tests and analysis have revealed detailed characteristics of the wheels and bearings, not indicating any increased wear. Simulations showed good correlation with wheel measurements. The influence of Eddy current losses on the overall characteristics has been clarified. Tests using the bearing cartridge alone identified their contribution to overall loss torque.
Further efforts in simulations will help to identify the remaining parts of the torque loss composition. A second endurance test with a slightly modified speed profile shall give a better understanding of stiction variations and further confidence in the new operation scheme.

References

[1] Harris, T.A., et al.(2007). *Roller Bearing Analysis 5th Edition: Essential Concepts of Bearing Technology*, CRC Press

[2] Hübner, J.M., et al.(2016). *Run, INTEGRAL, run! Low wheel speed operations for fuel savings*, SpaceOps 2016 Conference Daejeon, Korea

[3] Anwar, S. & Stevenson, R. (2006). *Torque Characteristics Analysis of an Eddy Current Electric Machine for Automotive Braking Applications*, IEEE, 3997